Supporting Information

Low-dimensional lateral heterojunctions made of hexagonal boron nitride and carbon materials as efficient electrocatalysts for chlorine evolution reaction: A study of DFT and machine learning

Jiake Fan, Lei Yang, Weihua Zhu*

Institute for Computation in Molecular and Materials Science, School of Chemistry and Chemical Engineering, Nanjing University of Science and Technology, Nanjing 210094, China

* Corresponding author. E-mail: zhuwh@njust.edu.cn

Table S1. The hyperparameters search space and the optimal hyperparameters of RFR

Hyperparameters	Search space	Optimal hyperparameters
n_estimators	(50,1000, step=50)	450
max_depth	(2, 18, step=2)	8

Table S2. The hyperparameters search space and the optimal hyperparameters of XGBR

Hyperparameters	Search space	Optimal hyperparameters
n_estimators	(40, 100, step=10)	100
max_depth	(3, 15, step=1)	13
min_child_weight	(5, 10, step=1)	5
colsample_bytree	(0.4, 1, step=0.1)	0.9
subsample	(0.4, 1, step=0.1)	0.9
reg_alpha	(0.1, 0.5, step=0.1)	0.1
reg_lambda	(0.5, 0.9, step=0.1)	0.7
gamma	(0, 1, step=1)	0

Table S3. The interaction energy between graphene and h-BN in lateral heterojunctions

Dimensional	Total energy/eV	The energy of h-BN/eV	The energy of graphene/eV	Interaction energy/eV
2	-33918.71665	-17317.97715	-16558.84154	-41.898
1	-63594.75111	-32492.86308	-31069.31618	-32.5719
0	-63479.5114	-30283.07519	-33098.76588	-97.6703

Table S4. Three groups of features

Group name	Features
Dimension	B fraction,

	C fraction, N fraction, sine coulomb matrix eig 4, sine coulomb matrix eig 5, sine coulomb matrix eig 7, sine coulomb matrix eig 8, sine coulomb matrix eig 9, sine coulomb matrix eig 10, sine coulomb matrix eig 11, sine coulomb matrix eig 12, sine coulomb matrix eig 13, sine coulomb matrix eig 14, sine coulomb matrix eig 15, sine coulomb matrix eig 18, sine coulomb matrix eig 19, sine coulomb matrix eig 20, sine coulomb matrix eig 21, sine coulomb matrix eig 22, sine coulomb matrix eig 23, sine coulomb matrix eig 24, sine coulomb matrix eig 25, Dimensions
Cl Concentration	Cl fraction, mean AtomicWeight, mean Column, mean Row,

	mean Number, mean AtomicRadius, mean Electronegativity, avg p valence electrons, frac s valence electrons, frac p valence electrons, sine coulomb matrix eig 0, sine coulomb matrix eig 1, sine coulomb matrix eig 2, sine coulomb matrix eig 3, sine coulomb matrix eig 6, sine coulomb matrix eig 32
Other	sine coulomb matrix eig 29 sine coulomb matrix eig 30 sine coulomb matrix eig 17 sine coulomb matrix eig 45 sine coulomb matrix eig 26 sine coulomb matrix eig 27 sine coulomb matrix eig 43 sine coulomb matrix eig 40 sine coulomb matrix eig 38 sine coulomb matrix eig 53 sine coulomb matrix eig 44 sine coulomb matrix eig 39 sine coulomb matrix eig 46 sine coulomb matrix eig 37

	sine coulomb matrix eig 58 sine coulomb matrix eig 34 sine coulomb matrix eig 54 sine coulomb matrix eig 35 sine coulomb matrix eig 48 sine coulomb matrix eig 57 sine coulomb matrix eig 49 sine coulomb matrix eig 47 sine coulomb matrix eig 59 sine coulomb matrix eig 56 sine coulomb matrix eig 31 sine coulomb matrix eig 52 sine coulomb matrix eig 36 sine coulomb matrix eig 55 sine coulomb matrix eig 51 sine coulomb matrix eig 41 sine coulomb matrix eig 60 sine coulomb matrix eig 16 sine coulomb matrix eig 33 sine coulomb matrix eig 50 sine coulomb matrix eig 42 sine coulomb matrix eig 28 sine coulomb matrix eig 61 sine coulomb matrix eig 62

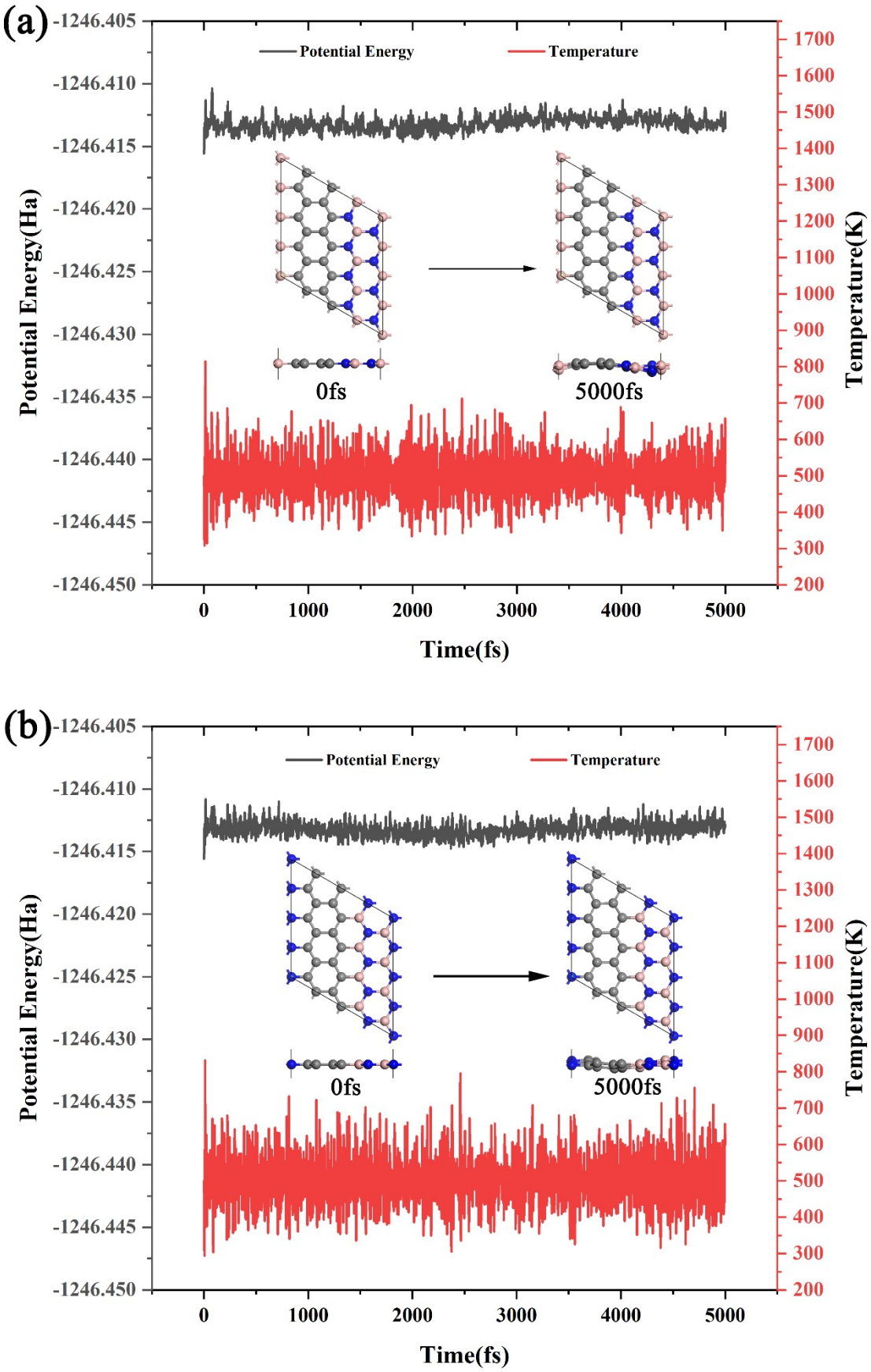

Figure S1. The Potential energy, temperature profiles and corresponding snapshots of G1 (a)

and G2 (b) based on AIMD

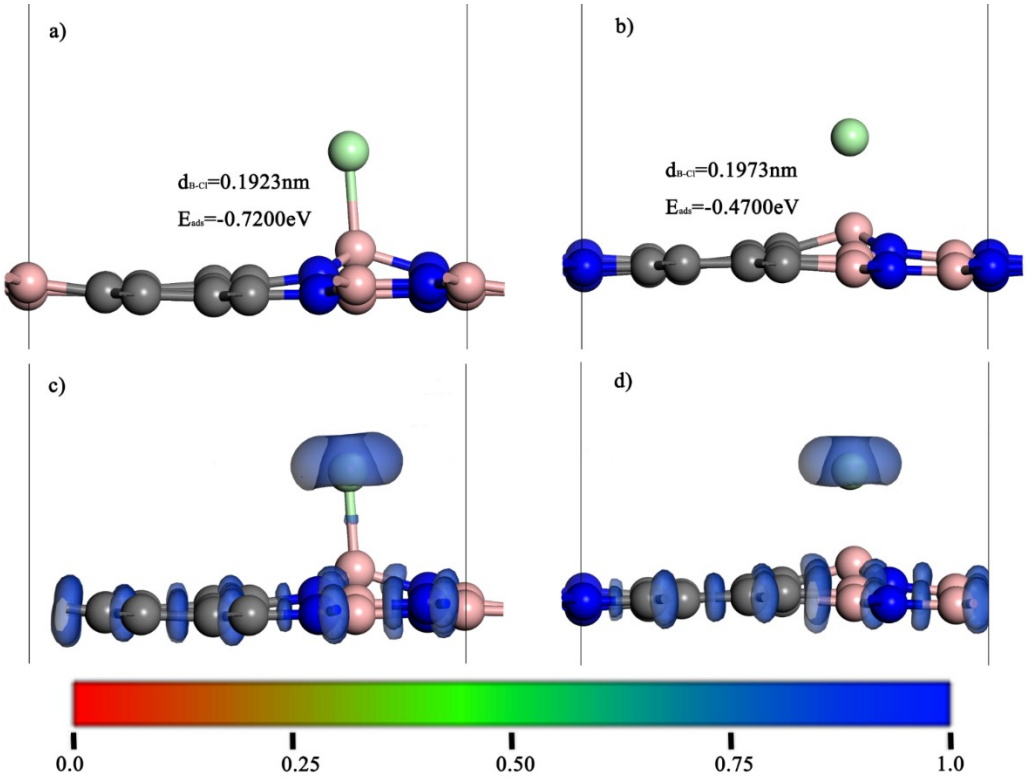

Figure S2. Length of d_{B-Cl} and binding energy of Cl^- adsorbed on G1 (a) and G2 (b), and electron localization function of G1 (c) and G2 (d).

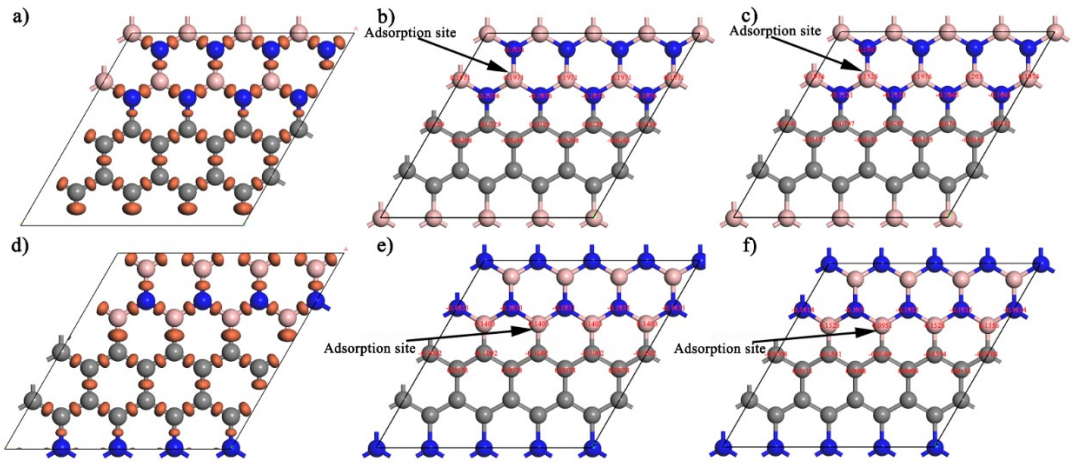

Figure S3. Electron localization function of G1 (a) and Hirshfeld charges of the atoms at the G1 interface before (b) and after (c) Cl^- adsorption. Electron localization function of G2 (d) and Hirshfeld charges of the atoms at the G2 interface before (e) and after (f) Cl^- adsorption.

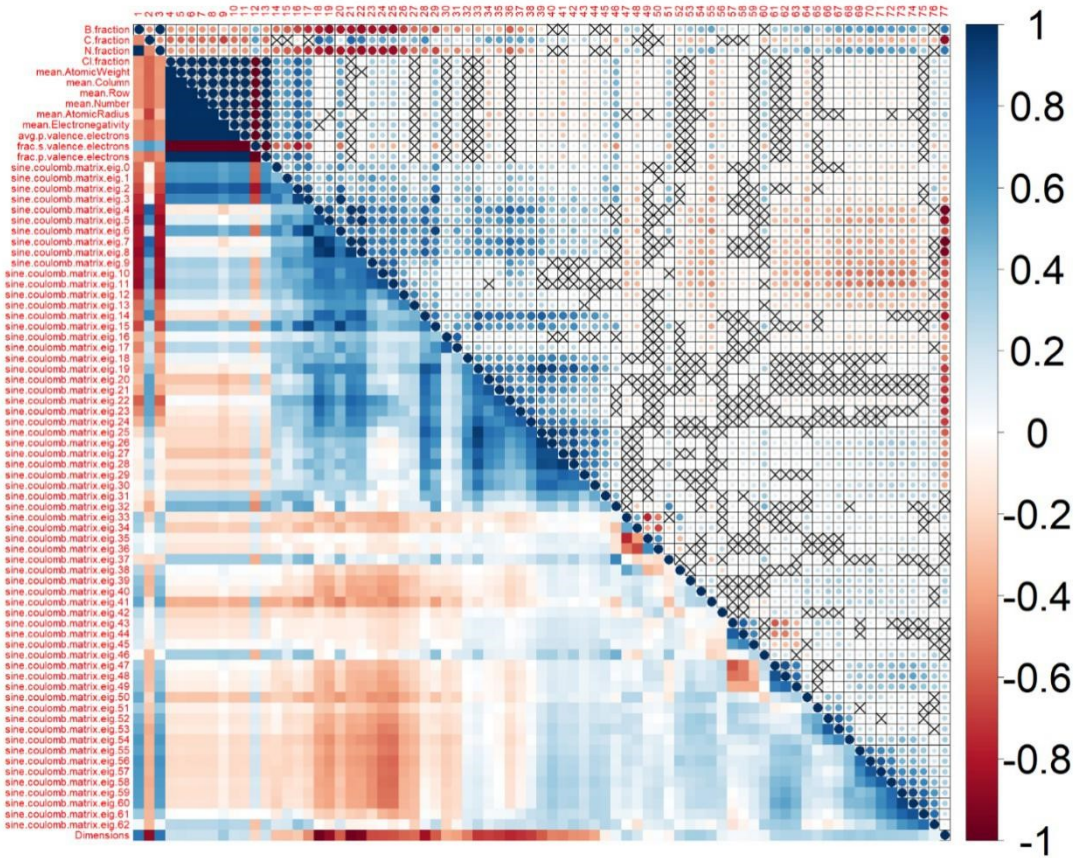
B.fraction
C.fraction
N.fraction
Cl.fraction
mean.AtomicWeight
mean.Column
mean.Row
mean.Number
mean.AtomicRadius
mean.Electronegativity
avg.p.valence.electrons
frac.s.valence.electrons
frac.p.valence.electrons
Dimensions
1
0.8
0.6
0.4
0.2
0
-0.2
-0.4
-0.6
-0.8
-1

(a)

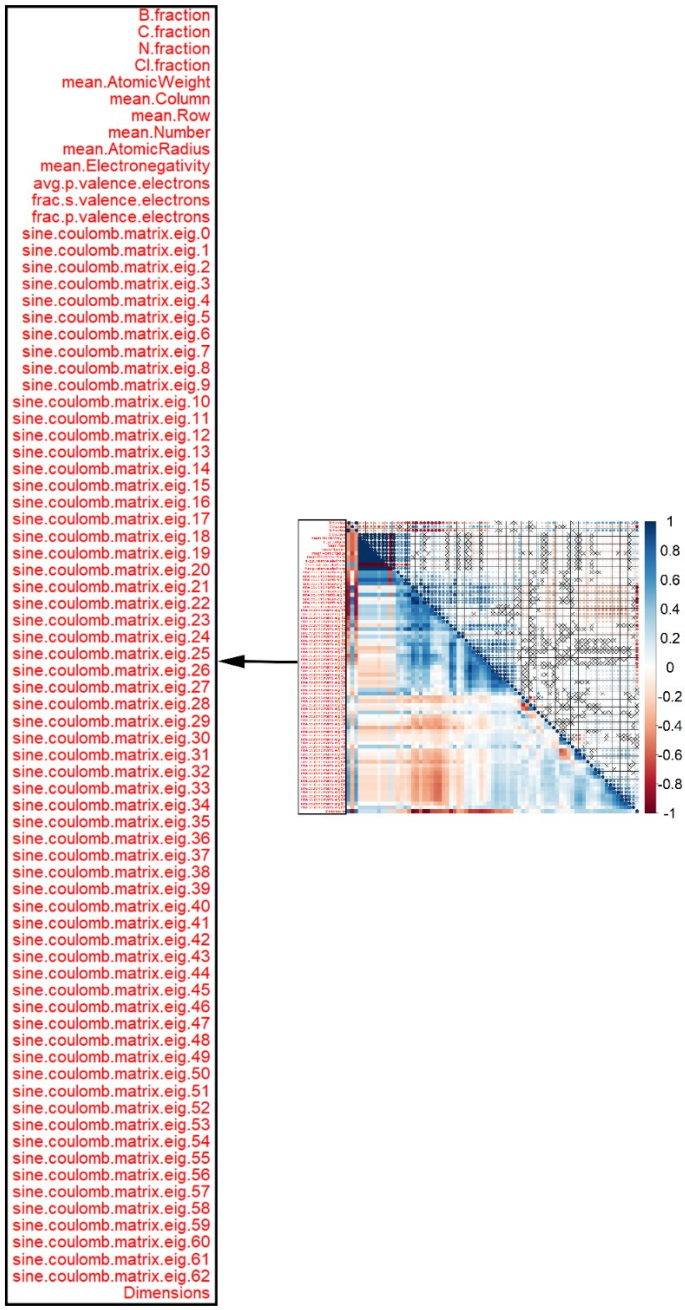

(b)

Figure S4. The heatmap of Pearson correlation coefficient and corresponding p-value between 77 features (the “x” in the grid indicates that there is no-significant-difference between two features; the larger the diameter of the circle and the darker the color, the greater the correlation between the two features) (a). The partial enlargement of the 77 feature labels(b).

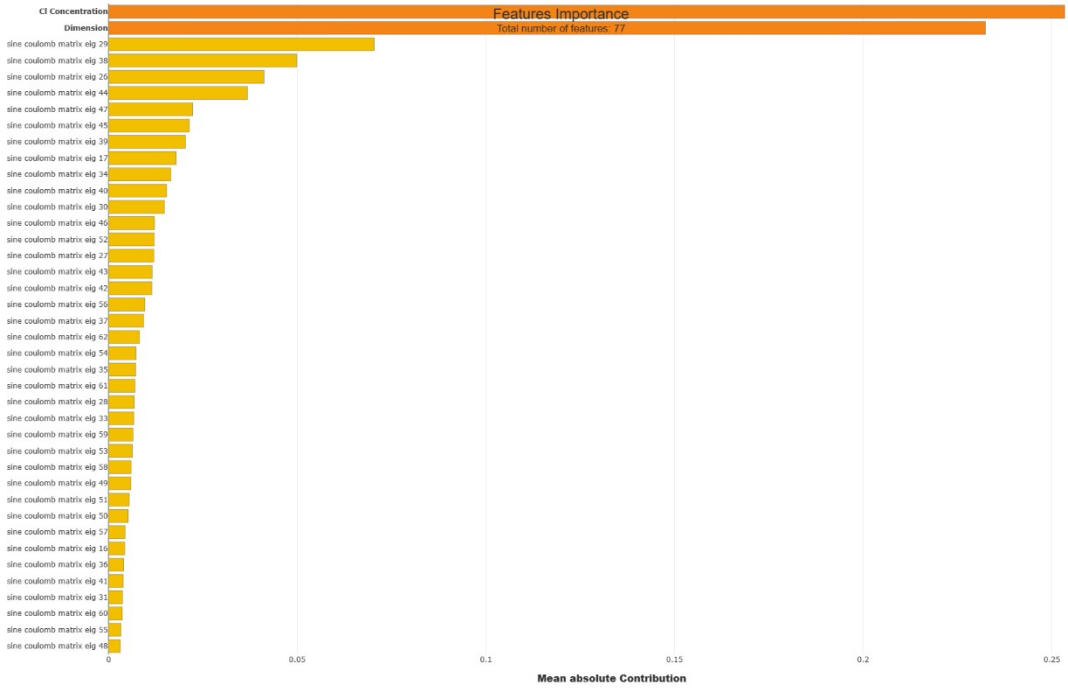

Figure S5. The SHAP feature importance calculated by the algorithm of RFR

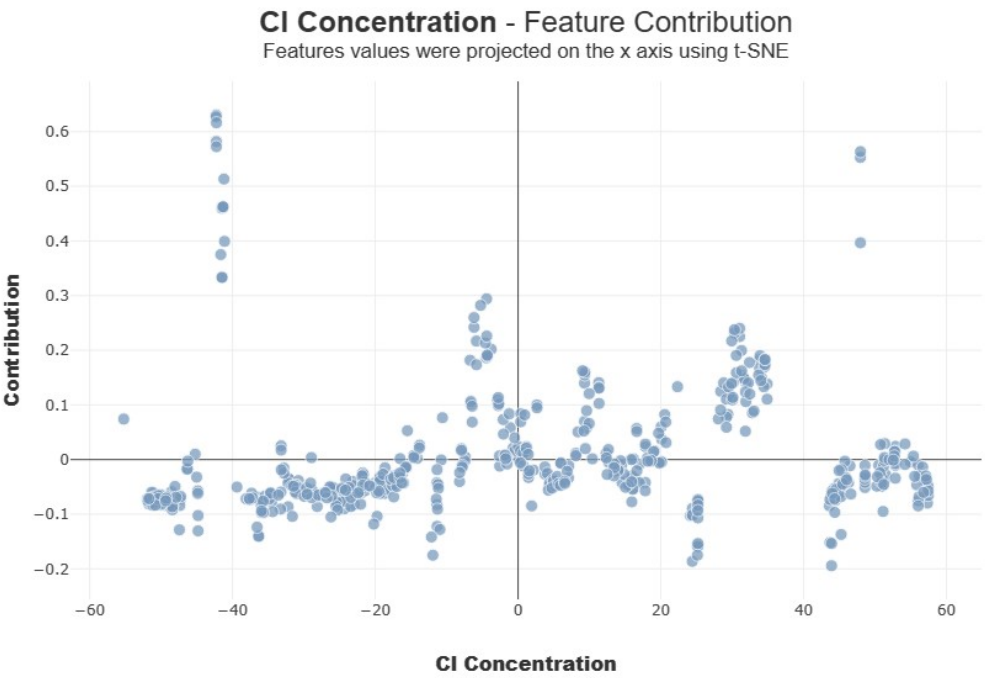

Figure S6. The c_{Cl}'s contribution to the ΔG_{CER} under the algorithm of RFR

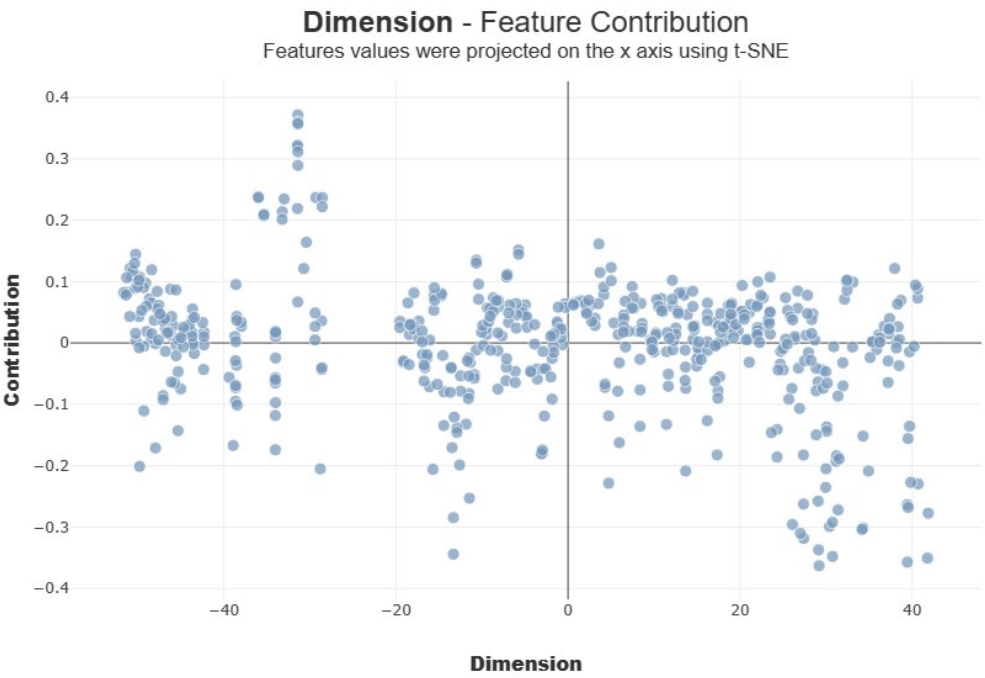

Figure S7. The contribution of heterojunction dimensions to the ΔG_{CER} under the algorithm of RFR

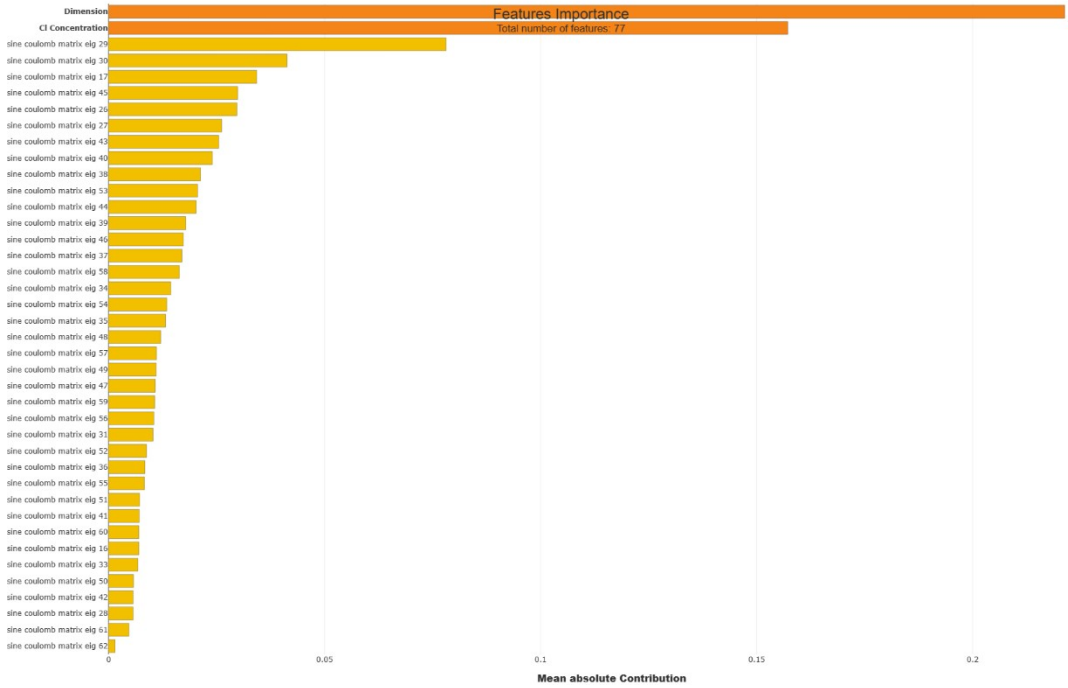

Figure S8. The SHAP feature importance under the algorithm XGBR

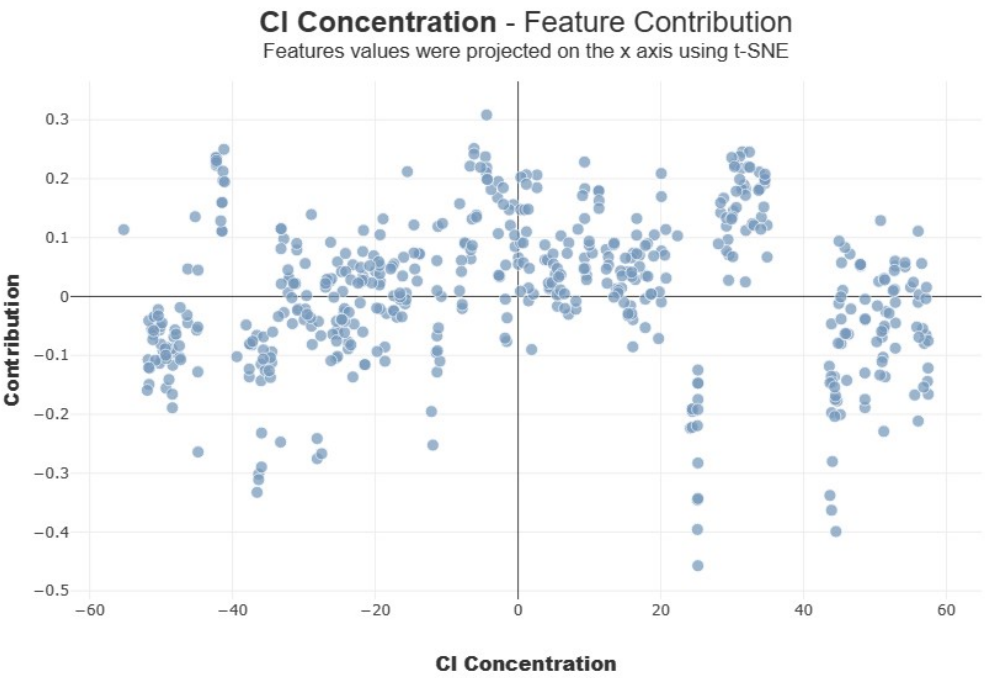

Figure S9. The c_{Cl}'s contribution to the ΔG_{CER} under the algorithm of XGBR

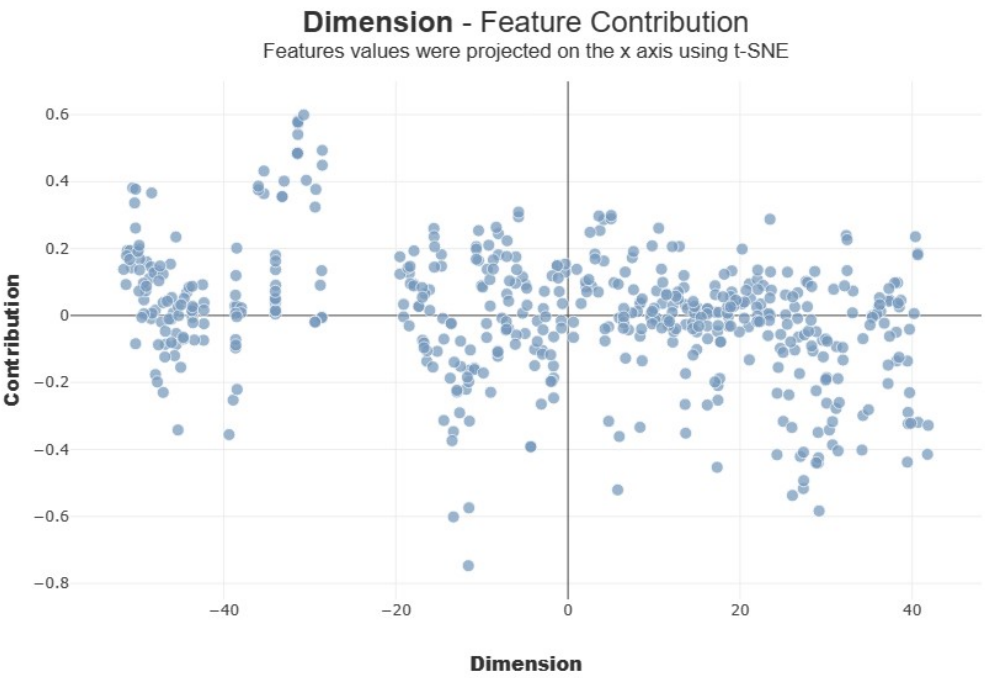

Figure S10. The contribution of heterojunction dimensions to the ΔG_{CER} under the algorithm of XGBR

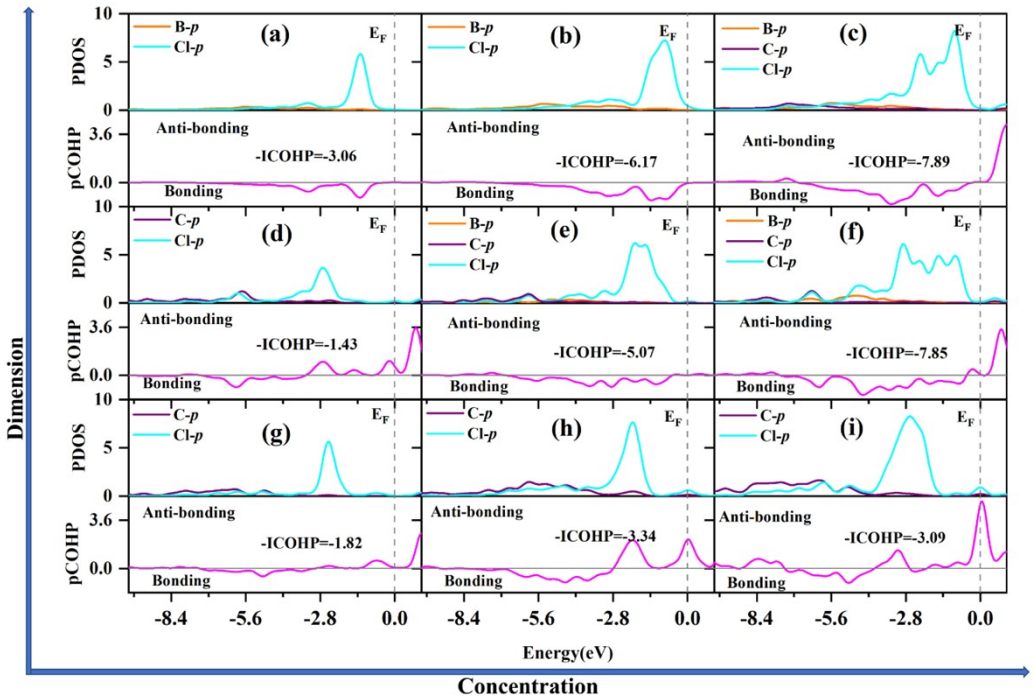

Figure S11. Partial density of states and projected crystal orbital Hamilton population (pCOHP) of the adsorption sites and Cl atoms under different surface coverage concentrations of Cl^- (c_{Cl}) and different heterojunction's dimensions (D) ((a) D=2, c_{Cl}=1; (b) D=2, c_{Cl}=2; (c) D=2, c_{Cl}=3; (d) D=1, c_{Cl}=1; (e) D=1, c_{Cl}=2; (f) D=1, c_{Cl}=3; (g) D=0, c_{Cl}=1; (h) D=0, c_{Cl}=2; (i) D=0, c_{Cl}=3).

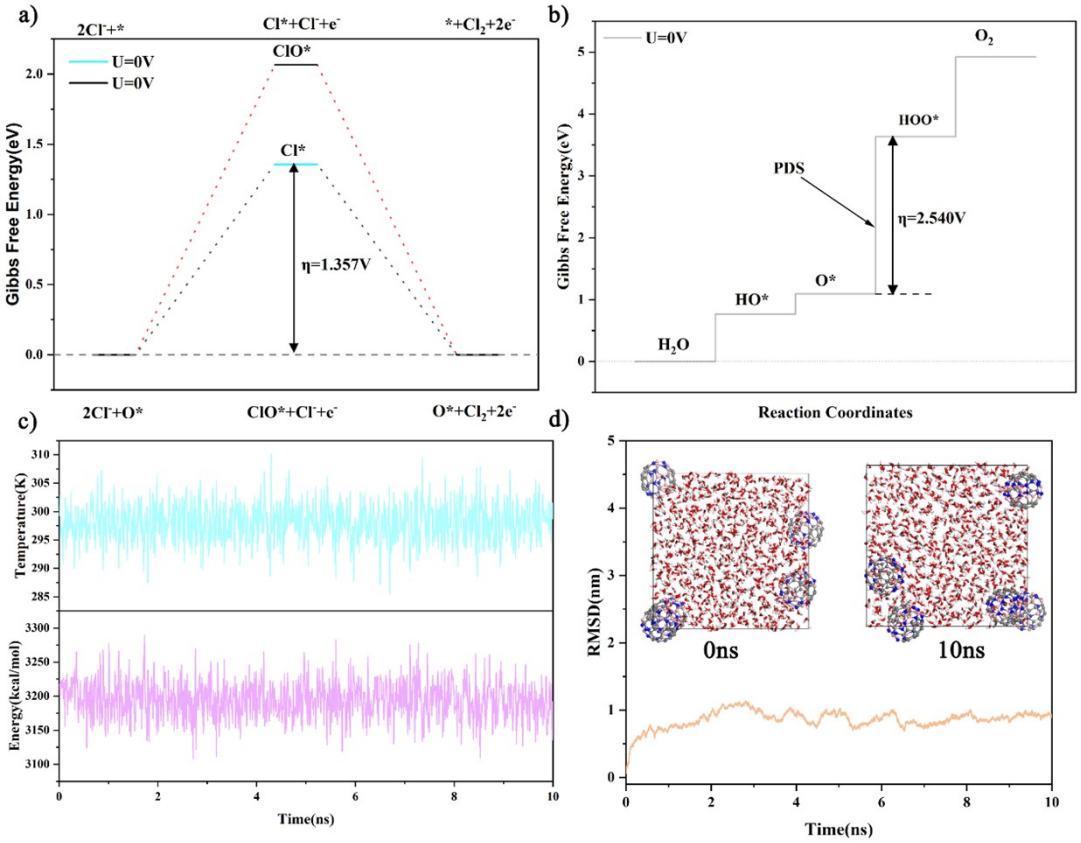

Figure S12. Gibbs free energy diagram of CER on the D_0_Cl5_C1_C2 (a) and OER on D_0_Cl5_C1_C2 (b) systems. Energy and temperature diagram (c) and root-mean-square deviation (RMSD) for zero-dimensional heterojunction in water and snapshots from molecular dynamics simulations (d).